AGU PUBLICATIONS

Geophysical Research Letters

RESEARCH LETTER
10.1002/2017GL074176

Key Points:
- The distribution of future sea level rise around Australia results from combination of ocean dynamics, loss of land ice, and GIA
- Dynamic sea level is the leading process to induce regional variations, under moderate and strong emission scenarios
- Downscaling with a 1/10° OGCM produces better dynamic sea level responses from climate models, linked to ocean gyre circulation

Supporting Information:
- Supporting Information S1

Correspondence to:
X. Zhang,
xuebin.zhang@csiro.au

Citation:
Zhang, X., J. A. Church, D. Monselesan, and K. L. McInnes (2017), Sea level projections for the Australian region in the 21st century, *Geophys. Res. Lett.*, *44*, 8481–8491, doi:10.1002/2017GL074176.

Received 31 MAY 2017
Accepted 29 JUL 2017
Accepted article online 2 AUG 2017
Published online 16 AUG 2017

Sea level projections for the Australian region in the 21st century

Xuebin Zhang[1], John A. Church[2], Didier Monselesan[3], and Kathleen L. McInnes[4]

[1]Centre for Southern Hemisphere Oceans Research (CSHOR), CSIRO Oceans and Atmosphere, Hobart, Tasmania, Australia, [2]Climate Change Research Centre, University of New South Wales, Sydney, New South Wales, Australia, [3]CSIRO Oceans and Atmosphere, Hobart, Tasmania, Australia, [4]CSIRO Oceans and Atmosphere, Aspendale, Victoria, Australia

Abstract Sea level rise exhibits significant regional differences. Based on Coupled Model Intercomparison Project Phase 5 (CMIP5) models, sea level projections have been produced for the Australian region by taking account of regional dynamic changes, ocean thermal expansion, mass loss of glaciers, changes in Greenland and Antarctic ice sheets and land water storage, and glacial isostatic adjustment. However, these regional projections have a coarse resolution (~100 km), while coastal adaptation planners demand finer scale information at the coast. To address this need, a 1/10° near-global ocean model driven by ensemble average forcings from 17 CMIP5 models is used to downscale future climate. We produce high-resolution sea level projections by combining downscaled dynamic sea level with other contributions. Off the southeast coast, dynamic downscaling provides better representation of high sea level projections associated with gyre circulation and boundary current changes. The high-resolution sea level projection should be a valuable product for detailed coastal adaptation planning.

1. Introduction

Contemporary sea level rise is an important indicator and measure of anthropogenic climate change. Global mean sea level (GMSL) has been rising according to tide gauge and satellite altimetry measurements and is projected to continue to rise in the future [e.g., *Meehl et al.*, 2007; *Church et al.*, 2013a; *Lyu et al.*, 2014]. Several physical processes can affect GMSL, including ocean thermal expansion, mass loss of glaciers and ice caps (GIC), changes in the Antarctic ice sheet (AIS) and the Greenland ice sheet (GIS), and changes in land water storage.

Sea level changes are not expected to be spatially uniform as several physical processes, such as ocean density and circulation change, loss of mass from land ice (GIC, AIS, and GIS), and glacial isostatic adjustment (GIA), all cause regional variations [e.g., *Slangen et al.*, 2012; *Church et al.*, 2013a]. The regional sea level distribution associated with contemporary loss of land ice (called sea level fingerprints) has been estimated by solving the sea level equation, in which effects of gravitation, solid-earth deformation, and rotation are all considered [*Farrel and Clark*, 1976; *Milne and Mitrovica*, 1996; *Mitrovica et al.*, 2011]. The melting of land ice (GIC, AIS, and GIS) generally induces a nonuniform sea level redistribution, with a sea level fall in the near fields and a greater than global average sea level rise in the far field [e.g., *Mitrovica et al.*, 2011]. In addition to regional sea level distribution associated with contemporary changes in land ice mass, there are also ongoing sea level changes associated with changes in surface loading over the last glacial cycle, the GIA [e.g., *Tamisiea and Mitrovica*, 2011]. Ocean density and circulation changes can also cause significant regional sea level distribution features. Dynamic sea level (DSL), the sea surface height relative to the Geoid, is determined by the dynamical balance associated with ocean density distribution and circulation. Global climate models provide useful information about the spatial patterns of DSL changes, though significant intermodel regional differences remain [e.g., *Yin*, 2012; *Slangen et al.*, 2015].

CMIP-type global climate models, with a relatively coarse spatial resolution (typical 1° resolution in the ocean), are primarily designed to study large-scale climate change and variability globally over decades to centuries. However, for local applications including climate adaption and mitigation planning, practitioners require much finer resolution at the coast—at least tens rather than 100 km [*Intergovernmental Panel for Climate Change* (*IPCC*), 2014]. Therefore, there are significant gaps in spatial resolution and reliability of climate information between what the state-of-the-art climate models provide and what the end users wish to obtain. How to fill such significant gaps is not only a cutting-edge research direction for regional climate

studies [e.g., *Xie et al.*, 2015] but also is urgently required for the development of localized adaptation and mitigation strategies [*IPCC*, 2014].

The CSIRO Ocean Downscaling Strategic Project (CODSP) is as an attempt to address these scale gaps using a near-global eddy-resolving (1/10°) ocean general circulation model (OGCM) to downscale ocean states for both the historical period and the 21st century projections of the ensemble average of 17 CMIP5 models under a high-emission scenario—Representative Concentration Pathways (RCP) 8.5 [*Zhang et al.*, 2016].

Australia is a large island nation, with about half of its population living within 7 km of the coast [*Chen and McAneney*, 2006]. Over the 21st century, sea levels around Australia are projected to rise [*McInnes et al.*, 2015]. The mean sea level rise will likely be felt through extreme sea level events, which lead to coastal flooding, inundation, and erosion [*Church et al.*, 2006; *McInnes et al.*, 2015]. Hence, careful planning, based on reliable projection of sea level rise, is critical for building resilience to sea level rise and adapting to its impacts.

To address the above need, we first produce projections of mean sea level around Australia based on the Fifth Assessment Report (AR5) of the IPCC [*Church et al.*, 2013a] and CMIP5 climate models [*Taylor et al.*, 2012]. We further examine how different sea level processes combine with each other to generate the total sea level projection with some interesting regional features around Australia. We then produce a unique high-resolution (1/10°) total sea level projection product, by combining the DSL derived from the downscaling with all other sea level contributions. Distinctive differences between coarse- and high-resolution projections and underlying dynamic processes are also examined.

2. Data Processing and Methodology

2.1. CMIP5 DSL Processing

We use sea surface height relative to the Geoid, the "ZOS" variable from CMIP5 models. The DSL, defined as regional sea level deviation from the global mean, is derived from "ZOS" with its time-dependent global mean removed [*Yin*, 2012; *Church et al.*, 2013a]. Projections of future climate change are defined with reference to the "present-day" mean state over 1986–2005. The artificial drift (i.e., spurious long-term changes) in historical and future experiments is estimated with a cubic polynomial fit to the corresponding control experiments of each individual climate model under constant preindustrial forcing, and is then removed [e.g., *Sen Gupta et al.*, 2013]. For this study, all four RCPs, i.e., 2.6, 4.5, 6.0, and 8.5, are considered to represent the low- to high-emission scenario range [*Edmonds et al.*, 2010]. Information about CMIP5 models, with slightly different ensemble sizes for four RCPs due to data availability, can be found in Table S1 in the supporting information. CMIP5 models have different horizontal grids, thus, regridding and ensemble averaging can lead to missing values in the coastal regions. To better preserve information from individual models and provide ensemble averages as close to the coastline as possible, each model is regridded to a common global 0.5° × 0.5° grid first, then any missing values close to the coastline are iteratively filled with values from the adjacent grid cells (left, right, upper and lower). Finally, multimodel ensemble averages are derived and used in the regional sea level projections (Figure S1 in the supporting information). Similar to the strategy of filling with nearest neighbor points used in the IPCC AR5 [*Church et al.*, 2013b], this mathematical in-filling technique provides a reasonable DSL distribution around Australia, although it is fundamentally different from the physics-based in-filling technique, used in the dynamical downscaling (section 2.3).

2.2. Regional Sea Level Projection

Only in recent years have total sea level projections at the regional scale been attempted [e.g., *Slangen et al.*, 2012, 2014; *Church et al.*, 2011, 2013a], with the basic idea that various sea level contributing processes can be linearly summed.

Our projections of regional sea level generally follow *Church et al.* [2011], by combining published GMSL contributions by the IPCC, and regional sea level contributions which include DSL processed by the CSIRO sea level group and various sea level fingerprints based on *Mitrovica et al.* [2011] (details of the projection methodology can be found in Text S1 in the supporting information [*Kendall et al.*, 2005]). One minor caveat is that the global mean contribution from land water storage change is included in our projection, but its regional contribution (deviation from the global mean) is not, since it is small (less than 1 cm) and quite uniform around Australia [*Slangen et al.*, 2014]. Overall our regional sea level projections under all RCPs are very similar

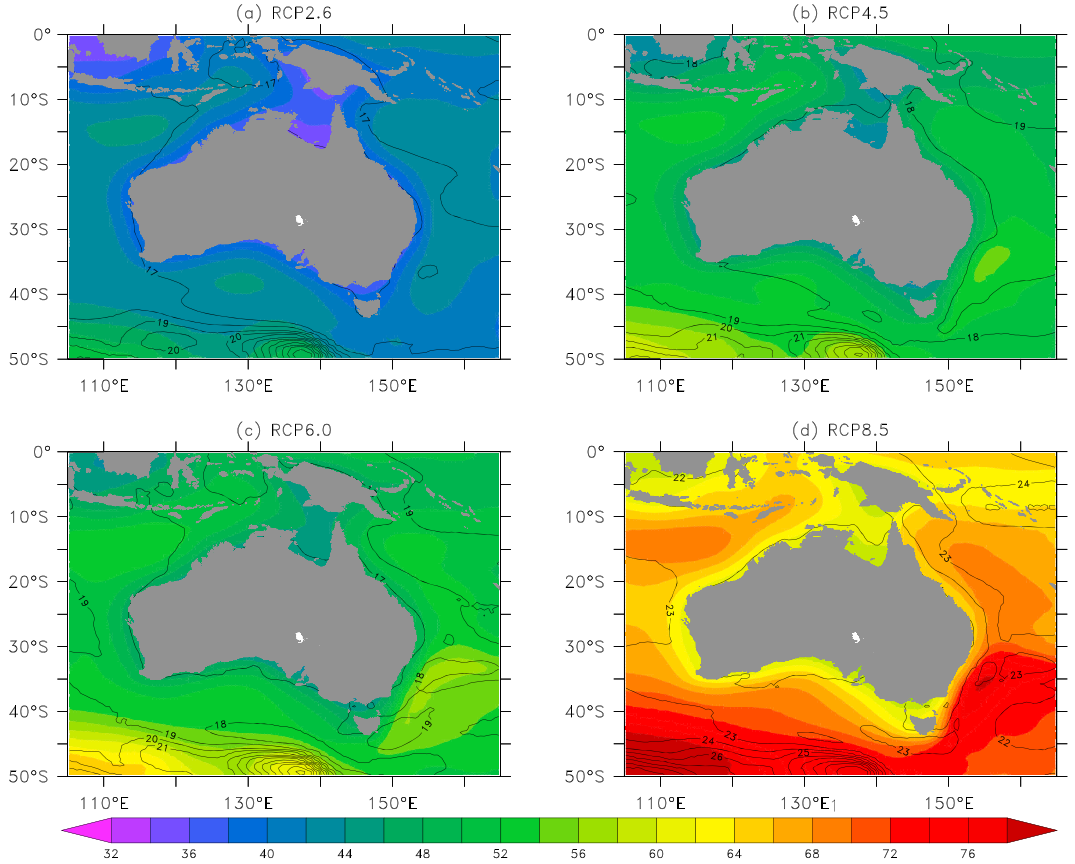

Figure 1. Total sea level projections (unit: cm) for the Australian region over 2080–2099 relative to 1986–2005 under four emission scenarios - RCP (a) 2.6, (b) 4.5, (c) 6.0, and (d) 8.5, with uncertainty indicated by contours.

(but not identical) to those reported in the IPCC AR5 [*Church et al.*, 2013a] and provide data closer to the coastline, mainly because of our tailored DSL processing (section 2.1).

2.3. High-Resolution Regional Sea Level Projections

Global high-resolution (sometimes referred to as "eddy resolving") ocean models are highly desired for climate studies, since they can simulate boundary currents and mesoscale eddies much better than coarse-resolution climate models, which play significant roles in heat transport and exchange [*Griffies et al.*, 2015], the ocean kinetic energy budget [*Ferrari and Wunch*, 2009; *Schiller et al.*, 2008]. However, global eddy-resolving ocean models are challenging to run, because they require careful configuration and substantial computational resources. In the CODSP, several strategies were developed so that a near-global high-resolution OGCM could be implemented for climate studies [*Zhang et al.*, 2016]. The OGCM used by the CODSP is affiliated with the Ocean Forecasting Australia Model Version 3 (OFAM3) [*Oke et al.*, 2013], which is based on version 4p1 of the GFDL Modular Ocean Model [*Griffies*, 2009] and configured to have 1/10° grid spacing for all longitudes between 75°S and 75°N, and 51 vertical layers.

After a 20 year spin-up with repeating year 1979 forcing, OFAM3 is integrated over 1979–2014 driven by JRA-55 reanalysis [*Kobayashi et al.*, 2015] through bulk formulas. Details about model setup, spin-up and historical experiments, and comprehensive validation with observations can be found in *Zhang et al.* [2016], and more information and regional validation plots can be found in Text S2 [*Danabasoglu et al.*, 1996; *Dee and Uppala*, 2009; *Kobayashi et al.*, 2015; *Maximenko et al.*, 2009; *Maltrud and McClean*, 2005; *Ridgway and Dunn*, 2003; *Yu et al.*, 2012] and Figures S5 and S6 in the supporting information [*Lumpkin and Johnson*, 2013]. These results demonstrate improved performance and greater details in the downscaled product. OFAM3 is further integrated to 2101, driven by merged atmospheric forcing fields which include the high-frequency (daily to

interannual) component from present-day JRA-55 reanalysis and long-term climate change signals from the ensemble of 17 CMIP5 models under RCP8.5 (details can be found in Text S2 in the supporting information). The consistently designed model runs (historical + future) from 1979 to 2101 provide high-resolution climate change projections for all ocean state variables, including sea level. Additionally, a control experiment with repeating 1979 year forcing that is run in parallel with the historical plus future experiments (1979 to 2101) is used to quantify artificial drifts, which we find are much smaller than the climate change signals and are removed from the corresponding historical and future experiments (see Figure S7 showing small drifts of sea level). Dedrifted high-resolution model results are thus used to estimate the "downscaled" changes in the ocean by comparing ocean states from the future experiment with reference to those in the historical experiment, similar to the CMIP5 model analysis.

The high-resolution DSL derived from the dynamical downscaling is then summed with all other sea level contributing processes to produce a high-resolution (1/10°) total sea level projection. This combination is based on the understanding that sea level fingerprints associated with the GIA and land ice mass loss (GIC, AIS, and GIS) induce large-scale responses, which for the "far-field" regions like Australia can be safely regridded to finer resolution [*Mitrovica et al.*, 2011]. The key difference between the high- and low-resolution total sea level projections is the DSL component, with the former coming from dynamical downscaling and the latter directly from CMIP5 models.

3. Regional Sea Level Projection Around Australia

Regional low-resolution sea level projections, derived from the ensemble of CMIP5 models around Australia over 2080–2099 relative to 1986–2005 under 4 RCP scenarios, are shown in Figure 1. Sea level rises are strongest under the business-as-usual scenario—RCP8.5 (Figure 1d), and weakest under the strong-mitigation scenario—RCP2.6 (Figure 1a), with intermediate values under the other two scenarios—RCPs 4.5 and 6.0 (Figures 1b and 1c). Projected sea level rise under RCP2.6 is about 40% of RCP8.5 as found through spatial regression analysis over the study region (105–165°E, 0–50°S), while the percentage is 58% and 74% under RCP4.5 and RCP6.0 relative to RCP8.5, respectively. The regional distribution of projected sea level rise is similar among RCPs 4.5, 6.0, and 8.5, with spatial correlation between any two scenarios higher than 0.95 over the study region. However, the regional distribution under RCP2.6 is slightly different to the other scenarios, with a lower spatial correlation of 0.78 between RCPs 2.6 and 8.5 (Figures 1a and 1d). The main reason for this is the higher sea levels off the southeast coast that are evident under all RCPs except RCP2.6. The spatial differences in total sea level projection are mainly due to differences in the DSL projection (see Figure S1 in the supporting information).

Using RCP8.5 as an example, we examine different regional sea level contributions in detail to provide a clear understanding how different sea level processes combine to produce the regional distribution of total sea level projections (Figure 2; also refer to Figures S2–S4 in the supporting information for other RCPs). Such examination was not done by previous studies [e.g., *Church et al.*, 2013a; *McInnes et al.*, 2015]. The DSL has high sea levels of 6–12 cm off the southeast coast of Australia, extending from ~30°S to 45°S (Figure 2a). There is a strong north-south contrast of DSL changes off the east coast, with smaller (higher) rise in the north (south). However, the north-south contrast of DSL mainly shows up offshore from the east coast, not along the coastline where there is a quite uniform DSL change of 3–4 cm (refer to Figure S8a in the supporting information). Along and off the Australian south coast, there are 2–4 cm negative DSL changes (negative deviation from the global average), with the maximum located just west of the Bass Strait. More negative DSL changes also extend to the southwest coast, implying a possible common underlying process (e.g., ocean gyre circulation as discussed in section 4). Along the Australian northwest and north coasts, the DSL changes are close to zero, although there is a zonal band of high DSL of 2 cm off the northwest coast, along 14°S from 105°E to 115°E.

Because Australia is in the far fields of the various fingerprints associated with loss of mass from the GIC, GIS, and AIS, the combined contributions from land ice mass change (Figure 2c) under RCP8.5 have quite smooth regional patterns around Australia. Along the Australian coastline, these contributions altogether cause 3 cm sea level rise (relative to their combined global means) except a slightly higher value (4 cm) along the southwest coast and slightly lower value (2 cm) in the Gulf of Carpentaria. A weak cross-shelf gradient with less than 1 cm higher sea level rise offshore than onshore mainly comes from the contribution from GIC

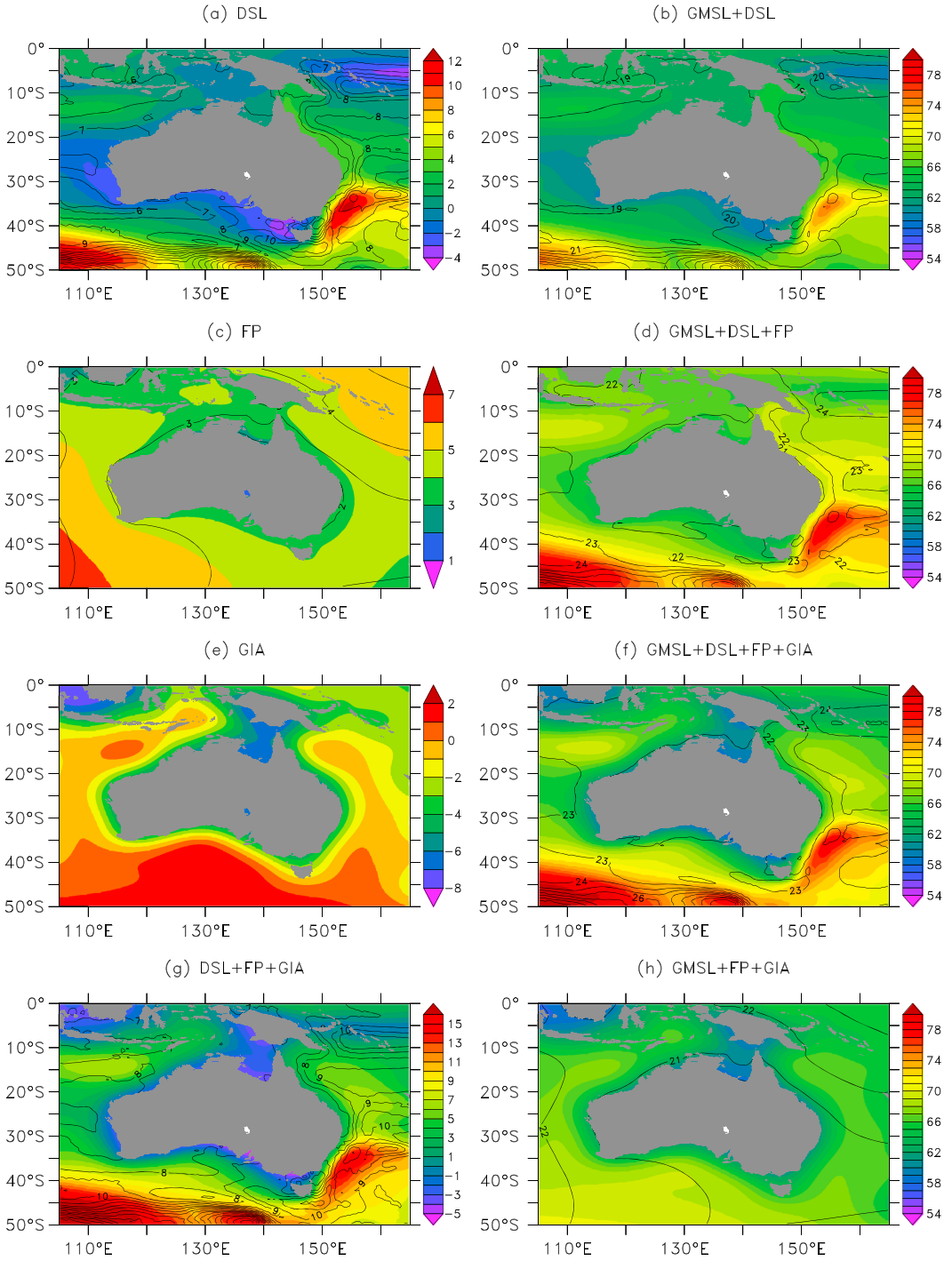

Figure 2. Left column shows projected regional sea level change (unit: cm) for the Australian region over 2080–2099 relative to 1986–2005 under RCP8.5 for (a) dynamic sea level (DSL), (c) sum of various regional sea level contributions due to land ice mass change (FP), (e) region sea level due to GIA, and (g) the sum of the previous three, i.e., DSL + FP + GIA. Right column shows several combinations of all global sea level contributions but with different regional sea level contributions: (b) GMSL + DSL, (d) GMSL + DSL + FP, (f) GMSL + DSL + FP + GIA, and (g) GMSL + FP + GIA. Uncertainty (unit: cm) is indicated by contours except (Figure 2e) for GIA where the uncertainty level is quite uniform ~2.5 cm. Detailed definitions of DSL, FP, and GIA and associated uncertainty can be found in the supporting information Text S1, in particular, the full expression of FP (termed as $\Delta F(x,y,t)$) is given there.

melting. The higher values in the southwest corner than the rest of the study region results from the combined contributions of surface mass balance (SMB) and rapid dynamical change of the AIS, with the former being projected to gain mass over the whole Antarctica, while the latter being projected to loss mass over the West Antarctica only [*Church et al.*, 2013a].

GIA not only induces a quite uniform local sea level fall of 3–4 cm along the Australian coastline, with a stronger fall (7 cm) in the Gulf of Carpentaria (Figure 2e), but also a stronger cross-shelf sea level gradient than the various sea level fingerprints combined (Figures 2c and 2e), with regional sea level varying from −3–4 cm onshore to near zero offshore.

By combing the above regional sea levels and all GMSL contributions, we get the total regional sea level projection under RCP8.5 (Figure 2f), which resembles the following intermediate sea level projections: GMSL contributions combined with DSL only (Figure 2b), and GMSL contributions combined with both DSL and various contributions of land ice (GIC, AIS, and GIS) (Figure 2d). The resemblance among them (Figures 2f, 2b, and 2d) indicates that the DSL contribution, common to all three, is the source of the regional variations. To first order, the regional distribution of total sea level is determined by the DSL under RCP8.5, as evidenced by a significant spatial correlation of 0.86 between Figures 2a and 2f. If the DSL contribution is excluded, the total sea level projection looks quite different, without significant regional differences around Australia, except in the Gulf of Carpentaria (Figure 2h).

Positive regional sea level contributions due to land ice mass changes (Figure 2c) tend to cancel out negative GIA-induced sea levels (Figure 2e), though the stronger cross-shelf gradient in GIA-induced sea level generally remains in the total sea level projection (Figures 2f and 2g).

The uncertainty of regional sea level projection, slightly larger for higher RCPs, is about 20 cm around Australia for all four RCPs, which is close to the uncertainty of GMSL projection (Figure 1) [*Church et al.*, 2013a]. Under RCP8.5, DSL leads to larger (~6–10 cm in Figure 2a) regional sea level projection uncertainty than land ice mass change (3–4 cm in Figure 2c) and GIA (~2.5 cm in Figure 2e) (see Text S1 for uncertainty definition).

The dominance of DSL determining regional distribution of total sea level projection as found under RCP8.5 is less obvious for the other RCPs, since the scenario-independent GIA contribution becomes comparable or even larger than the scenario-dependent DSL contribution under weaker RCPs, especially under the weakest RCP2.6 (Figure S2 in the supporting information). In summary, the total sea level projection around Australia is the result of a complex combination of various regional and global sea level processes, which have some scenario dependence.

4. High-Resolution Sea Level Projection Around Australia Based On Downscaled DSL

As discussed above, the DSL is the main process determining the regional distribution of sea level projection around Australia under moderate to high scenarios. Because CMIP climate models do not have sufficient spatial resolution, tailored data-processing procedures, in particular, the mathematical in-filling technique, have to be carefully designed to provide information up to the coast (section 2.1). Dynamic downscaling directly addresses this problem and provides a dynamic (and physically consistent) method based on the high-resolution model physics.

The large-scale DSL distribution over 2080–2099 has similar patterns between coarse- and high-resolution products under RCP8.5 (Figures 3a and 3b), but the high-resolution downscaled DSL reveals detailed regional features, which are absent in the coarse-resolution DSL. In particular, there is a narrow meridional band of high sea levels of 20–30 cm immediately off the southeast coast, extending from ~30°S to 45°S. This regional distribution barely shows up in the coarse-resolution product, although smooth high sea levels with a maximum slightly above 10 cm can be found further offshore (see maps in Figures 3a and 3b and also the zonal distribution along 36°S off the southeast coast in Figure S9 in the supporting information).

Despite large differences off the coast, the differences between the coarse- and high-resolution DSL changes along the Australian coastline are quite small (1–3 cm), with the high-resolution product showing a stronger asymmetry between positive DSL changes along the east and negative DSL changes along the southwest

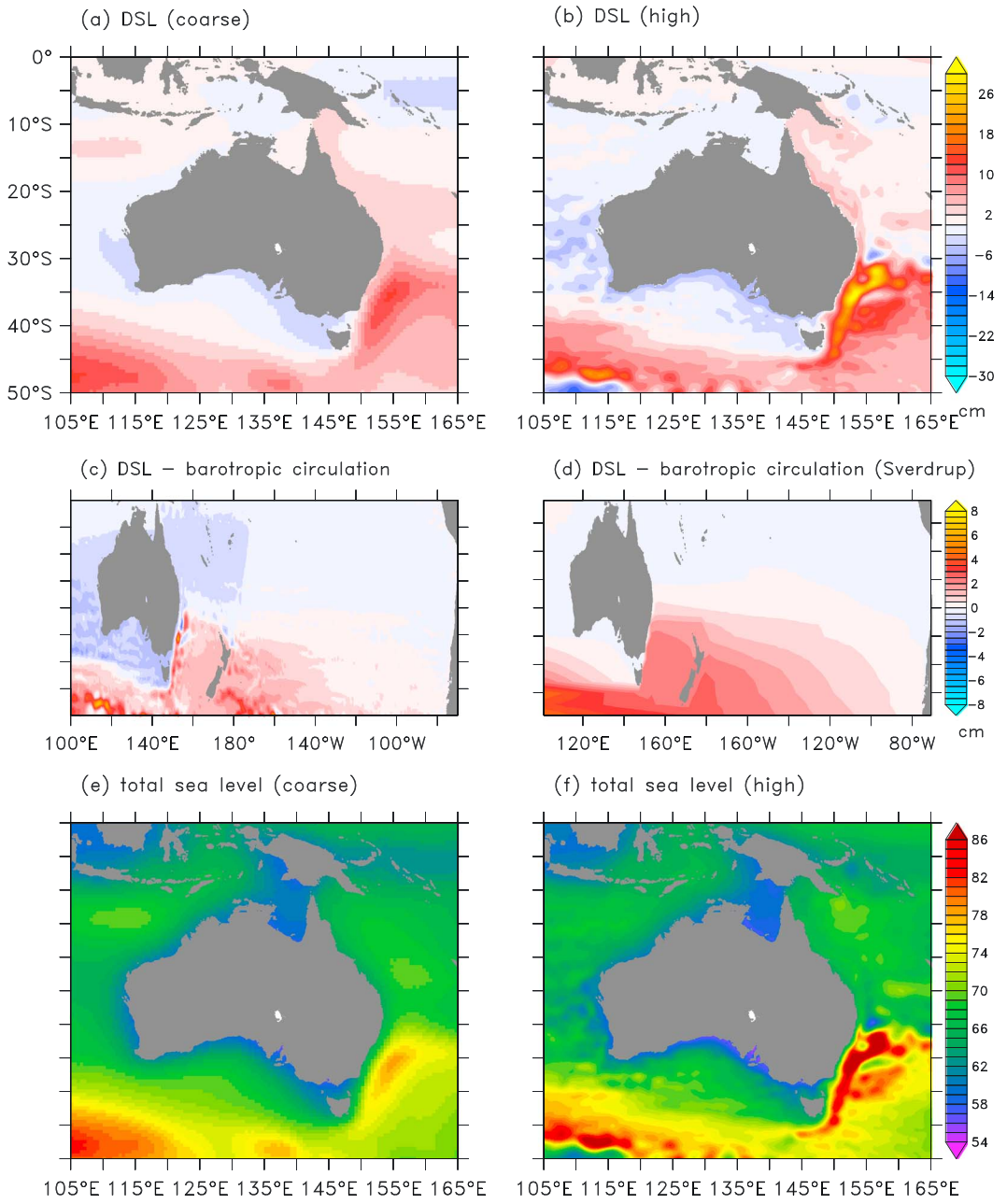

Figure 3. Dynamical sea level (DSL) change (unit: cm) under RCP8.5 over 2080–2099 relative to 1986–2005, for the Australian region (a) from coarse-resolution CMIP5 ensemble and (b) the high-resolution downscaled product. DSL change (unit: cm) associated with barotropic circulation (equation (1)) based on stream function change (c) directly integrated from ocean velocity and (d) indirectly calculated from wind stress based on the Sverdrup Balance and the Island Rule. Total sea level change (unit: cm) under RCP8.5 over 2080–2099 relative to 1986–2005, including all global and regional contributions with (e) Coarse-resolution (0.5°) DSL and (f) high-resolution (0.1°) DSL. Figures 3a, 3b, 3e, and 3f are intentionally plotted to show its natural grids, i.e., 0.5° in Figures 3a and 3e and 0.1° in Figures 3b and 3f without interpolation.

and south coasts (see Figure S8 in the supporting information). Smaller DSL changes along the coastline can be roughly understood by considering zero norm-flow requirement on the coastline and geostrophic balance, which implies a weak alongshore (i.e., tangential) sea level gradient, although a detailed momentum balance analysis is necessary to get an in-depth understanding of sea level and ocean currents along the Australian coast, which is to be carried out in a follow-up study.

Compared to other coasts around the world, the DSL change signals are relatively small (within ±6 cm) along the Australian coastline. The differences between high-resolution and low-resolution projections along the Australian coastline are even smaller (within ±3 cm), since the high-resolution projections come from dynamical downscaling, which by its design is meant to get detailed climate information constrained by large-scale input from parent climate models [*Flato et al.*, 2013]. However, the above situation of small sea level changes and small differences does not apply everywhere around the world. For example, there are much larger differences (>10 cm) between high- and coarse-resolution results elsewhere (to be reported in a follow-up global study).

Without the DSL contribution, the total sea level projections have a much smoother spatial distribution, with quite uniform value along the coastline, as well as only a weak cross-shelf gradient (Figure 2h). Including the DSL contribution dramatically increases regional diversity in both low- and high-resolutions (Figures 3e and 3f). The contrast between low- and high-resolution DSL is well demonstrated in the contrast between two total sea level projections (see Figures 3a, 3b, 3e, and 3f). The mixing of low-resolution fingerprints with high-resolution DSL should be treated as an intermediate step toward high-resolution total sea level projections, but as we have shown here, it is an appropriate and straightforward solution to get high-resolution total sea level projections especially for "far-field" regions (i.e., far away from the sources of land ice mass loss).

The regional distribution of DSL with relatively high (low) sea levels off the southeast coast (south and southwest coast) of Australia in both high- and low-resolution models is closely related to ocean circulation changes in the future (Figure 3). The dominant feature is that the subtropical gyres in the Southern Hemisphere are projected to strengthen and shift poleward, the so-called "supergyre spin-up" [*Ridgway and Dunn*, 2007; *Cai et al.*, 2010], which occurs in response to the poleward expansion of subtropical highs of sea level pressure and associated strong and consistent anticyclonic wind stress curl forcing changes between 35° and 50°S in the South Pacific [*Zhang et al.*, 2014].

For ease of understanding, assume there is a barotropic circulation in the ocean basin. DSL is connected to the stream function through the following relationship:

$$\eta_{\mathrm{bc}} = \frac{f}{gH}\psi \tag{1}$$

where η_{bc} is DSL associated with barotropic circulation, f the Coriolis parameter, g acceleration of gravity, H the mean water depth (assumed as 4000 m), and ψ the stream function, which can be either directly integrated from ocean velocity or indirectly calculated from wind stress based on the Sverdrup Balance and the Island Rule [*Sverdrup*, 1947; *Godfrey*, 1989].

In the South Pacific, η_{bc} (Figures 3c and 3d) tends to intensify westward from the South American continent. Such westward intensification, a well-known feature in ocean gyre circulation, can be understood by zonal integration of wind stress curl forcing across the South Pacific basin. So the DSL changes around Australia, such as high (low) sea levels off the southeast coast (south and southwest coast) are not just regional distributional features but rather part of basin-scale oceanic changes in response to changes of atmospheric forcing (especially wind forcing).

The η_{bc} tends to have higher (smaller) values in higher (lower) latitudes (Figures 3c and 3d) because of the latitude-dependence of the Coriolis parameter (equation (1)). The η_{bc} can explain the DSL quite well south of 30°S, with very good spatial correspondence but smaller magnitudes. Larger η_{bc} of several centimeters can be found immediately off the southeast coast of Australia, where larger DSLs are located. The discrepancy of magnitudes between DSL and η_{bc} simply reflects that the assumption of barotropic circulation is only a crude approximation. In fact, although consistent circulation patterns tend to penetrate from the surface to middepth around 2000 m in the South Pacific subtropical gyre, ocean circulation is surface intensified rather than vertically uniform [*Roemmich et al.*, 2007; *Zhang et al.*, 2014]. Nonetheless, equation (1) adequately explains the associated changes of sea level and ocean gyre circulation.

The different representation of the high DSL changes off the southeast coast between high and low resolution can also be understood by the different representation of the western boundary current (WBC), which is

an essential element of ocean gyre circulation. The cross-shelf slope of sea level in the WBC regions is generally in geostrophic balance with WBC transport [e.g., *Thompson and Mitchum*, 2014; *Ezer et al.*, 2013]. With 1/10° horizontal resolution, OFAM3 can represent the WBC systems realistically, as validated with satellite and drifter observations [*Oke et al.*, 2013; *Zhang et al.*, 2016; *Feng et al.*, 2016]. On the contrary, climate models cannot adequately simulate the observed narrow WBCs, nor represent mesoscale eddies and the associated high eddy kinetic energy. The sharp and narrow DSL changes off the southeast coast from the high-resolution simulation are closely related to the stronger EAC Extension in the future climate [*Sun et al.*, 2012] (Figure 3b, also refer to Figure S9 in the supporting information).

5. Summary and Discussion

In this study, we presented total sea level projections around Australia by the end of the 21st century and examined how different contributing processes combine together to determine regional sea levels. We found that among several regional processes, the dynamic sea level is the dominant term under moderate to strong scenarios leading to high sea level deviations, on the order of 20–30 cm in the high-resolution projection compared to approximately 10 cm in the low-resolution projection offshore from the southeast coast of Australia under RCP8.5. The combination of the scenario-independent contribution from GIA and scenario-dependent contribution from dynamic sea level and sea level contributions due to land ice mass loss leads to a complicated regional distribution of sea level rise around Australia, with some dependence on emission scenarios.

The high-resolution sea level projection is based on the technique of dynamical downscaling [e.g., *Giorgi et al.*, 2001; *Flato et al.*, 2013], which uses global climate model as an input to a finer resolution model to obtain improved regional climate information. Our dynamic downscaling with a 1/10° OGCM can provide consistent projections of many ocean state variables (including sea level, ocean temperature, and currents) and underlying physical processes, at a much finer scale ($<$10 km) and closer to the coastline than the global climate models. The better representation of ocean gyre circulation and western boundary currents and their impacts on sea level projections around Australia as reported here is a clear demonstration of the benefit of dynamic downscaling.

As reported in *White et al.* [2014], GIA is not the only process to cause vertical land motion around Australia. Local factors, such as ground water extraction, can induce nontrivial vertical land motions, which are not included in our current study, though they should be included in local studies.

As a large island country with most of the population living near the coast, Australia will be significantly impacted by sea level rise. Hence, careful consideration, based on reliable projections of regional sea level rise such as this study, is critical for informing coastal adaptation and mitigation. We are working to extend this Australia-focused analysis to a global study, in particular, for those low-lying regions of the Earth.

Acknowledgments
CMIP5 model data are downloaded from the PCMDI (http://www-pcmdi.llnl.gov). The downscaling results are produced by the CSIRO Ocean Downscaling Strategic Project, in close collaboration with the Bluelink team (http://wp.csiro.au/bluelink/global/). Downscaling experiment was carried out at the Australian National Computing Infrastructure (NCI, http://nci.org.au/), and data presented in this paper are available upon request through the corresponding author. We also thank A. Slangen, R. Van de Wal, and two anonymous reviewers for their critical comments. This work is supported by the Earth System and Climate Change Hub of Australian Government's National Environmental Science Programme and the New South Wales Government through its Environmental Trust (2014/RD/0038).

References

Cai, W., T. Cowan, S. Godfrey, and S. Wijffels (2010), Simulations of processes associated with the fast warming rate of the southern midlatitude ocean, *J. Clim.*, *23*, 197–206.

Chen, K., and J. McAneney (2006), High-resolution estimates of Australia's coastal population, *Geophys. Res. Lett.*, *33*, L16601, doi:10.1029/2006GL026981.

Church, J. A., J. R. Hunter, K. L. McInnes, and N. J. White (2006), Sea-level rise around the Australian coastline and the changing frequency of extreme sea-level events, *Aust. Meteorol. Mag.*, *55*, 253–260.

Church, J. A., J. M. Gregory, N. J. White, S. M. Platten, and J. X. Mitrovica (2011), Understanding and projecting sea level change, *Oceanography*, *24*, 130–143, doi:10.5670/oceanog.2011.33.

Church, J. A., et al. (2013a), Sea level change, in *Climate Change 2013: The Physical Science Basis. Contribution of Working Group I to the Fifth Assessment Report of the Intergovernmental Panel on Climate Change*, edited by T. F. Stocker et al., pp. 1137–1216, Cambridge Univ. Press, Cambridge, U. K., and New York.

Church, J. A., et al. (2013b), Sea level change supplementary material, in *Climate Change 2013: The Physical Science Basis. Contribution of Working Group I to the Fifth Assessment Report of the Intergovernmental Panel on Climate Change*, edited by T. F. Stocker et al., pp. 1–8, Cambridge, Univ. Press, Cambridge, U. K., and New York.

Danabasoglu, G., J. C. McWilliams, and W. G. Large (1996), Approach to equilibrium in accelerated global oceanic models, *J. Clim.*, *9*, 1092–1110.

Dee, D. P., and S. Uppala (2009), Variational bias correction of satellite radiance data in the ERA-interim reanalysis, *Q. J. R. Meteorol. Soc.*, *135*, 1830–1841, doi:10.1002/qj.493.

Edmonds, J. A., et al. (2010), The next generation of scenarios for climate change research and assessment, *Nature*, *463*, 747–756.

Ezer, T., L. P. Atkinson, W. B. Corlett, and J. L. Blanco (2013), Gulf Stream's induced sea level rise and variability along the U.S. mid-Atlantic coast, *J. Geophys. Res. Oceans*, *118*, 685–697, doi:10.1002/jgrc.20091.

Farrel, W. E., and J. A. Clark (1976), On postglacial sea level, *Geophys. J. R. Astron. Soc.*, *46*, 647–667.

Feng, M., X. Zhang, P. Oke, D. Monselesan, M. Chamberlain, R. Matear, and A. Schiller (2016), Invigorating ocean boundary current systems around Australia during 1979-2014 – As simulated in a near-global eddy-resolving ocean model, *J. Geophys. Res. Oceans*, *121*, 3395–3408, doi:10.1002/2016JC011842.

Ferrari, F., and C. Wunch (2009), Ocean circulation kinetic energy: Reservoirs, sources, and sinks, *Annu. Rev. Fluid Mech.*, *41*, 253–282.

Flato, G., et al. (2013), Evaluation of climate models, in *Climate Change 2013: The Physical Science Basis. Contribution of Working Group I to the Fifth Assessment Report of the Intergovernmental Panel on Climate Change*, edited by T. F. Stocker et al., pp. 741–866, Cambridge Univ. Press, Cambridge, U. K., and New York.

Giorgi, F., et al. (2001), *Regional Climate Information–Evaluation and Projections. Climate Change 2001: The Scientific Basis*, edited by J. T. Houghton et al., pp. 583–638, Cambridge Univ. Press, Cambridge, U. K., and New York.

Godfrey, J. S. (1989), A Sverdrup model of the depth-integrated flow for the world ocean allowing for island circulations, *Geophys. Astrophys. Fluid Dyn.*, *45*, 89–112, doi:10.1080/03091928908208894.

Griffies, S. M. (2009), Elements of MOM4p1, GFDL Ocean Group Technical Report 6, Tech. Rep., NOAA/Geophys. Fluid Dyn. Lab.

Griffies, S. M., et al. (2015), Impacts on ocean heat from transient mesoscale eddies in a hierarchy of climate models, *J. Clim.*, *28*, 952–977.

Intergovernmental Panel on Climate Change (2014), Summary for policymakers, in *Climate Change 2014: Impacts, Adaptation, and Vulnerability. Part A: Global and Sectoral Aspects. Contribution of Working Group II to the Fifth Assessment Report of the Intergovernmental Panel on Climate Change*, edited by C. B. Field et al., pp. 1–32, Cambridge Univ. Press, Cambridge, U. K., and New York.

Kendall, R. A., J. X. Mitrovica, and G. A. Milne (2005), On post-glacial sea level. II. Numerical formulation and comparative results on spherically symmetric models. *Geophys. J. Int. 161*, 679–706, doi:10.1111/j.1365-246X.2005.02553.x.

Kobayashi, S., et al. (2015), The JRA-55 reanalysis: General specifications and basic characteristics, *J. Meteorol. Soc. Jpn.*, *93*, 5–48, doi:10.2151/jmsj.2015-001.

Lumpkin, R., and G. C. Johnson (2013), Global ocean surface velocities from drifters: Mean, variance, El Niño–Southern Oscillation response, and seasonal cycle, *J. Geophys. Res. Oceans*, *118*, 2992–3006, doi:10.1002/jgrc.20210.

Lyu, K., X. Zhang, J. A. Church, A. B. A. Slangen, and J. Hu (2014), Time of emergence for regional sea-level change, *Nat. Clim. Change*, *4*, 1006–1010, doi:10.1038/NCLIMATE2397.

Maltrud, M. E., and J. L. McClean (2005), An eddy resolving global 1/10° ocean simulation, *Ocean Model.*, *8*, 31–54, doi:10.1016/j.ocemod.2003.12.001.

Maximenko, N., P. Niiler, L. Centurioni, M.-H. Rio, O. Melnichenko, D. Chambers, V. Zlotnicki, and B. Galperin (2009), Mean dynamic topography of the ocean derived from satellite and drifting buoy data using three different techniques. *J. Atmos. Ocean. Technol.*, *26*, 1910–1919, doi:10.1029/2011JC007573.

McInnes, K. L., J. A. Church, D. Monselesan, J. R. Hunter, J. G. O'Grady, I. D. Haigh, and X. Zhang (2015), Information for Australian impact and adaptation planning in response to sea-level rise, *Austr. Meteorol. Oceanogr. J.*, *65*(1), 127–149.

Meehl, G., et al. (2007), Global climate projections, in *Climate Change 2007: The Physical Science Basis*, edited by S. Solomon et al., pp. 747–845, Cambridge Univ. Press, Cambridge.

Milne, G. A., and J. X. Mitrovica (1996), Postglacial sea-level change on a rotating earth: First results from a gravitationally self-consistent sea-level equation, *Geophys. J. Int.*, *126*, F13–F20.

Mitrovica, J. X., N. Gomez, E. Morrow, C. Hay, K. Latychev, and M. E. Tamisiea (2011), On the robustness of predictions of sea level fingerprints, *Geophys. J. Int.*, *187*, 729–742.

Oke, P. R., D. A. Griffin, A. Schiller, R. J. Matear, R. Fiedler, J. Mansbridge, A. Lenton, M. Cahill, M. A. Chamberlain, and K. Ridgway (2013), Evaluation of a near-global eddy-resolving ocean model, *Geosci. Model Dev.*, *6*, 591–615, doi:10.5194/gmd-6-591-2013.

Roemmich, D., J. Gilson, R. Davis, P. Sutton, S. Wijffels, and S. Riser (2007), Decadal spinup of the South Pacific subtropical gyre, *J. Phys. Oceanogr.*, *37*, 162–173.

Ridgway, K. R., and J. R. Dunn (2003), Mesoscale structure of the mean East Australian Current System and its relationship with topography, *Progress Oceanogr.*, *56*, 189–222.

Ridgway, K. R., and J. R. Dunn (2007), Observational evidence for a southern hemisphere oceanic supergyre, *Geophys. Res. Lett.*, *34*, L13612, doi:10.1029/2007GL030392.

Schiller, A., P. R. Oke, G. Brassington, M. Entel, R. Fiedler, D. A. Griffin, and J. V. Mansbridge (2008), Eddy-resolving ocean circulation in the Asian–Australian region inferred from an ocean reanalysis effort, *Prog. Oceanogr.*, *76*, 334–365.

Sen Gupta, A., N. C. Jourdain, J. N. Brown, and D. Monselesan (2013), Climate drift in the CMIP5 models, *J. Clim.*, *26*, 8597–8615, doi:10.1175/JCLI-D-12-00521.1.

Slangen, A. B. A., et al. (2012), Towards regional projections of twenty-first century sea-level change based on IPCC SRES scenarios, *Clim. Dyn.*, *38*, 1191–1209, doi:10.1007/s00382-011-1057-6.

Slangen, A. B. A., et al. (2014), Projecting twenty-first century regional sea-level changes, *Clim. Change*, *124*, 317–332, doi:10.1007/s10584-014-1080-9.

Slangen, A. B. A., J. A. Church, X. Zhang, and D. P. Monselesan (2015), The sea level response to external forcings in historical simulations of CMIP5 climate models, *J. Clim.*, *28*, 8521–8539.

Sun, C., M. Feng, R. J. Matear, M. A. Chamberlain, P. Craig, K. R. Ridgway, and A. Schiller (2012), Marine downscaling of a future climate scenario for Australian boundary currents, *J. Clim.*, *25*, 2947–2962, doi:10.1175/JCLI-D-11-00159.1.

Sverdrup, H. U. (1947), Wind-driven currents in a baroclinic ocean: With application to the equatorial currents in the eastern Pacific, *Proc. Natl. Acad. Sci.*, *33*, 318–326.

Tamisiea, M. E., and J. X. Mitrovica (2011), The moving boundaries of sea level change: Understanding the origins of geographic variability, *Oceanography*, *24*, 24–39, doi:10.5670/oceanog.2011.25.

Taylor, K. E., R. J. Stouffer, and G. A. Meehl (2012), An overview of CMIP5 and the experiment design, *Bull. Am. Meteorol. Soc.*, *93*, 485–498, doi:10.1175/BAMS-D-11-00094.1.

Thompson, P. R., and G. T. Mitchum (2014), Coherent sea level variability on the North Atlantic western boundary, *J. Geophys. Res. Oceans*, *119*, 5676–5689, doi:10.1002/2014JC009999.

White, N. J., et al. (2014), Australian sea levels – Trends, regional variability and influencing factors, *Earth-Sci. Rev.*, *136*, 155–174, doi:10.1016/j.earscirev.2014.05.011.

Xie, S.-P., et al. (2015), Towards predictive understanding of regional climate change, *Nat. Clim. Change*, *5*, 921–930.

Yin, J. (2012), Century to multi-century sea-level rise projections from CMIP5 models, *Geophys. Res. Lett.*, *39*, L17709, doi:10.1029/2012GL052947.

Yu, Y., H. Liu, and P. Lin (2012), A quasi-global 1/10 eddy-resolving ocean general circulation model and its preliminary results, *Chin. Sci. Bull.*, doi:10.1007/s11434-012-5234-8.

Zhang, X., J. A. Church, S. M. Platten, and D. Monselesan (2014), Projection of subtropical circulation and associated sea-level changes in the Pacific ocean based on CMIP3 climate models, *Clim. Dyn.*, *43*, 131–144, doi:10.19007/s00382-013-192-x.

Zhang, X., P. Oke, M. Feng, M. Chamberlain, J. Church, D. Monselesan, C. Sun, R. Matear, A. Schiller, and R. Fiedler (2016), A near-Global Eddy-Resolving OGCM for Climate Studies, *Geosci. Model Dev. Discuss.*, doi:10.5194/gmd-2016-17.